



A hybrid method for pavement crack width measurement

Jeremy C.H. Ong¹, Mohd-Zulhilmi Paiz Ismadi¹, Xin Wang^{*}

School of Engineering, Monash University Malaysia, Subang Jaya 47500, Malaysia

ARTICLE INFO

Keywords:

Width measurement
Crack quantification
Asphalt pavement
Orthogonal projection

ABSTRACT

Accurate crack width measurement is crucial to determine the severity level of pavement cracks and the selection of crack repair strategy. We propose to combine the shortest method with the orthogonal projection method to produce a novel hybrid method. The hybrid method obtains the crack width by identifying a pair of points that give the shortest distance while being close to the orthogonal direction. We tested quantitatively and qualitatively the shortest, orthogonal projection and the hybrid methods on images taken from our CrackSkel700 dataset and two other open datasets, CrackForest, and Crack500. For the qualitative test, one hundred manual measurements are taken randomly from five images in the datasets to compare the shortest, orthogonal projection and hybrid methods on real cracks. Compared to the shortest and orthogonal projection methods, the hybrid method obtains the least root mean squared (RMS) error of 1.000 pixels and the least absolute pixel deviation of 0.732 pixels. Then, we generated 30 synthetic cracks using circles with a known diameter ranging from 3 pixels to 61 pixels to evaluate the accuracy of each method. The synthetic cracks generated a total of 18,404 ground truth measurements. Based on the synthetic cracks, the hybrid method obtains the least average absolute deviation of 1.769 pixels and the highest correlation coefficient of 0.956 compared to the shortest and orthogonal projection method on synthetic cracks. The qualitative comparisons of real and synthetic cracks show that the hybrid method improves the shortest method significantly by reducing the number of repeated measurements. On the other hand, the hybrid method improves the orthogonal projection method by reducing the overestimation of non-parallel and high curvature cracks. Hence, we show that the hybrid method generalizes better to more crack patterns and thus produces more accurate crack width estimation than the orthogonal projection and the shortest method.

1. Introduction

Road pavements and highways play a crucial role in economic development. Road networks connect citizens from every corner of the country and provide access to employment, healthcare, education, and other essential services. As the road network expands, it becomes difficult to address pavement distresses such as cracks and potholes. These pavement distresses are formed due to the constant application of traffic loads and environmental factors [1,2]. The most common type of distress found on pavements is cracks, and they can be generalized into three types: traverse, longitudinal, and alligator cracks. The presence of cracks removes the water-proofing capability of the road and allows water to seep into the roadbed, thus weakening the overall structure [3]. More serious distresses are formed such as potholes due to the weaker roadbed and the constant application of traffic loads [4]. A survey conducted by Lee et al. showed that poor pavement conditions contributed to 16% of the total accidents in 2015 [5].

Crack detection has been a popular topic for many years. The advancement of image processing technology allowed researchers to develop crack detection methods that produce accurate crack segmentation maps [6–11]. However, obtaining an accurate crack segmentation map only shows the location of the crack but does not explain the severity of the crack. The severity of the crack is defined by the characteristics of the crack, such as crack length, width, depth, and spacing. To assess the severity of the crack, transportation agencies still employ well-trained operators to obtain quantitative measurements of the crack, such as crack length, width, and spacing. Operators who conduct manual measurements can only obtain a few measurements [12]. This manual measurement is inconsistent as the crack length and width are often subjected to the operator's experience. This directly affects the accuracy of crack length and width measurement [13].

Crack quantification can be separated into two categories: semi-automatic and automatic methods. Semi-automatic methods refer to the process of detection through an image acquisition system. After

* Corresponding author.

E-mail address: wang.xin@monash.edu (X. Wang).

acquiring the images, an operator must analyze, evaluate, and judge the severity of the crack. Automatic methods refer to analyzing, identifying, and judging cracks based on image processing algorithms [14].

Semi-automatic methods such as crack scale and crack seeds are simple but slow. For example, the crack scale method proposed by Yamaguchi et al. requires the operator to place a crack scale near the crack while the photo is taken so that the algorithm can interpolate the crack width based on the crack scale [15]. The crack seed method requires the operator to go through the crack images and place random points along the crack to measure the average width [16].

So far, many researchers have employed the averaging method to obtain the average crack width, but this method downplays the severity of the crack [17–19]. Hence, researchers started to measure the crack width at every point to provide more accurate information about the crack width. Chun et al. proposed that the width of a crack is the shortest distance between the two boundaries to the skeleton pixel [20]. Benz et al. proposed to transform the gray-scale crack pixel distribution into an equal area rectangular shape to obtain the width of the crack [21]. These methods do not consider the propagation direction of a crack and, as a result, underestimate the width of the crack.

Then, researchers incorporate the crack propagation direction to obtain a better crack width estimate. Jahanshashi et al. developed a method that uses predefined strip kernels. The orientation of the crack is determined by the minimum correlation value. Once the orientation is found, the crack width is obtained by finding the ratio of the area bounded by the strip kernel and the crack segmentation to the tangential length [12]. Takafumi et al. measured the width of a crack by first interpolating the skeleton using a cardinal spline interpolation technique. Then the orientation of the crack is obtained based on the derivative of the interpolated curve. The distance is obtained by finding the points which intersect with the orthogonal direction [22]. Converting discrete pixels to continuous values using the spline interpolation method gives high fluctuations to the spline at high order polynomials and thus provides inaccurate orientation of the crack. Duan et al. developed a crack width method via cascade principal component analysis. This method uses Principal Component Analysis to determine the orientation of the crack without relying on the skeleton of the crack. Then, the crack width is the distance where the orthogonal vector and the segmentation mask intersects [23]. Shi et al. developed the orthogonal projection method to measure the crack width at every skeleton pixel. Then, contours are formed based on the boundary points to simplify the crack geometry. The distance is the Euclidean distance between the intersecting points of the orthogonal ray and the simplified contour [24]. Wang et al. developed a segment-based crack width measurement method based on the assumption that a small segment of the crack has parallel boundaries. The width is measured by translating the skeleton to the boundaries [13]. Ni et al. proposed a method based on Zernike-moment to measure thin cracks on concrete [25]. Kim et al. estimate the crack width by finding the Euclidean distance where the normal line intersects with the boundary pixels [26]. Payab et al. proposed to use a graph-based technique on crack images to obtain characteristics of a graph. The method obtains the crack orientation by using the central difference scheme based on the skeleton points. Then a line is extended by 0.1 pixel interval along the normal direction until it exceeds the crack boundary [27].

Wang et al. proposed to model the crack width based on Laplace's equation where each pixel in one boundary corresponds to another pixel in the opposing boundary. The crack width is the distance between the two points based on their trajectory [28].

Based on the methods discussed above, one limitation of the shortest method proposed by Chun et al. is that it underestimates the crack width, as the method is easily skewed by jagged edges of the crack boundary [20]. On the other hand, the disadvantage of using the orthogonal projection proposed by Shi et al. is that the method overestimates the crack width at unparallel boundaries and cracks with high curvatures [24].

Higher crack width measurement accuracy is needed as the crack width is used to determine a suitable crack repair strategy and material, directly affecting crack repair cost and time. For example, it is found that cracks that have widths 0.5 mm and below do not require immediate repair but should be monitored as external substances such as water and de-icing salt can accelerate crack growth [29]. On the other hand, crack sealing, or filling can repair cracks ranging from 0.5 mm to 40 mm depending on the pavement type and guidelines established by different countries. Other strategies should be used for cracks that cannot be repaired using the crack sealing or filling strategy, such as patching, surface dressing, and others [30–34]. In addition, outliers in crack width measurement should be reduced as this affects the autonomy of crack width measurement and selection of crack repair strategy.

Based on the guidelines provided by transportation agencies, obtaining a more accurate crack width is crucial in determining a suitable crack repair strategy and selection of materials [30–34]. Therefore, we propose to combine the shortest method and the orthogonal projection method to produce a novel hybrid method to improve the accuracy of crack width estimation. The proposed hybrid method obtains the shortest distance between a group of nearly orthogonal points to the crack propagation direction. The novelty of our method lies in the combination of the two methods.

2. Implementation of existing methods

We reimplemented the two most popular methods: the shortest and the orthogonal projection methods suggested by Chun et al. and Shi et al., respectively [20,24]. The details of the implementation are described in Sections 2.1 and 2.2.

2.1. Shortest method

The shortest method proposed by Chun et al. locates two points that lie on opposing sides that are closest to the skeleton point [20]. The boundary points of the crack are obtained using the Canny edge detector. Then, the orthogonal vector is obtained using a constant kernel size of five. The orthogonal vector is used to split the boundary points into two groups by obtaining the projection coefficients of the boundary points with respect to the orthogonal vector. The points with a positive projection coefficient lie ahead of the skeleton point and are thus grouped together. The points with a negative projection coefficient lie behind the skeleton point and are grouped together. Hence, the points of each group lie opposing each other. For each group, the point which gives the minimum distance to the skeleton point is found. Then, the crack width is the Euclidean distance between the two points. An illustration of the shortest method is shown in Fig. 1(a). The advantage of using the shortest method is that it is robust to pixel shift in the skeleton. The disadvantage of using the shortest method is that the algorithm does not consider the crack propagation direction. In turn, the measurement is easily skewed by the jagged edges of a crack, as seen in Fig. 1(b). Therefore, the shortest method underestimates the crack width and sometimes obtains repeated measurements using different skeleton points.

2.2. Orthogonal projection method

The orthogonal projection method proposed by Shi et al. locates two points closest to the orthogonal vector [24]. First, the boundary points of the crack are obtained by using the Canny edge detector. The orthogonal projection method uses a constant kernel size of five to determine the orthogonal vector. Once the orthogonal vector is found, the boundary points are projected onto the orthogonal vector to obtain the projection coefficients. The maximum and minimum projection coefficients indicate the two points that lie closest to the orthogonal vector but are opposite of each other. Then, the distance is obtained by calculating the Euclidean distance between the two points. The process of the

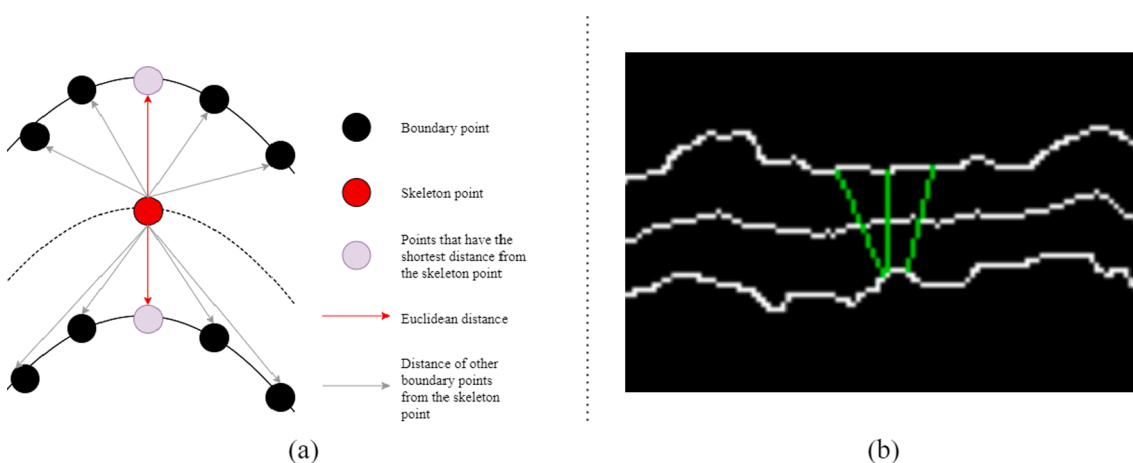


Fig. 1. (a) Illustration of crack width obtained using the shortest method. (b) Skewed measurement due to jagged edges.

orthogonal projection method is illustrated in Fig. 2(a). The advantage of using the orthogonal projection method is that it takes account into the crack propagation direction. The disadvantage of using the orthogonal projection method is that it sometimes chooses boundary points not directly in front or behind the skeleton point. This error occurs because of the boundary pixels' discrete values and the selection of boundary points that lie closest to the orthogonal vector. Another disadvantage of using the orthogonal projection method is that it is very sensitive to pixel shift in the skeleton. These disadvantages cause the orthogonal projection method to overestimate the crack width, as seen in Fig. 2(b).

3. Methodology

3.1. Crack skeleton extraction

To understand the geometry of the crack, the skeleton of the crack is first obtained. A skeleton describes the geometry of any shape. Therefore, an accurate skeleton representation is essential to measure the length and width of any shape. There are several ways to obtain the skeleton of a crack [35–37]. In this paper, Medial Axis Transform (MAT) proposed by Blum et al. is used, as it has the ability to reconstruct the original shape, which will be useful to measure the importance of each end branch and to locate local boundary points [38].

A skeleton point obtained by MAT is the center of the maximal disk. A maximal disk is tangent to the boundary in at least two points not

found in any other disks. Due to the jagged boundaries of a crack, the skeleton produced by MAT contains many spurious branches. These spurious branches create false intersections that do not accurately describe the crack's shape. This can affect the accuracy of crack length and width measurements. Therefore, we adapted a skeleton pruning algorithm known as Discrete Skeleton Evolution (DSE) developed by Bai et al. to remove these spurious branches [39].

The DSE first obtains the unpruned skeleton and the distance transform matrix via MAT. The distance transform matrix stores the radius of the maximal disk at each skeleton point, $s \in S$. The reconstructed shape $R(S)$ is obtained by merging the disks at each skeleton point with its corresponding radius, r , as shown in Equation (1), where function D is the function for rasterizing a disk given its midpoint and radius.

$$R(S) = \bigcup_{s \in S} D(s_i, r_i)) \quad (1)$$

Then, the end branches, E of a skeleton, are found by identifying edges with a degree of one. Each end branch is assigned a weight, w , by identifying the number of unique pixels that each end branch contributes to the reconstructed shape. The weights of each end branch obtained are shown in Equation (2).

$$w_i = \sum_j^n \left(R(S)_j > 0 \right) \oplus \left(\left(R(S)_j - E_{ij} \right) > 0 \right) \quad (2)$$

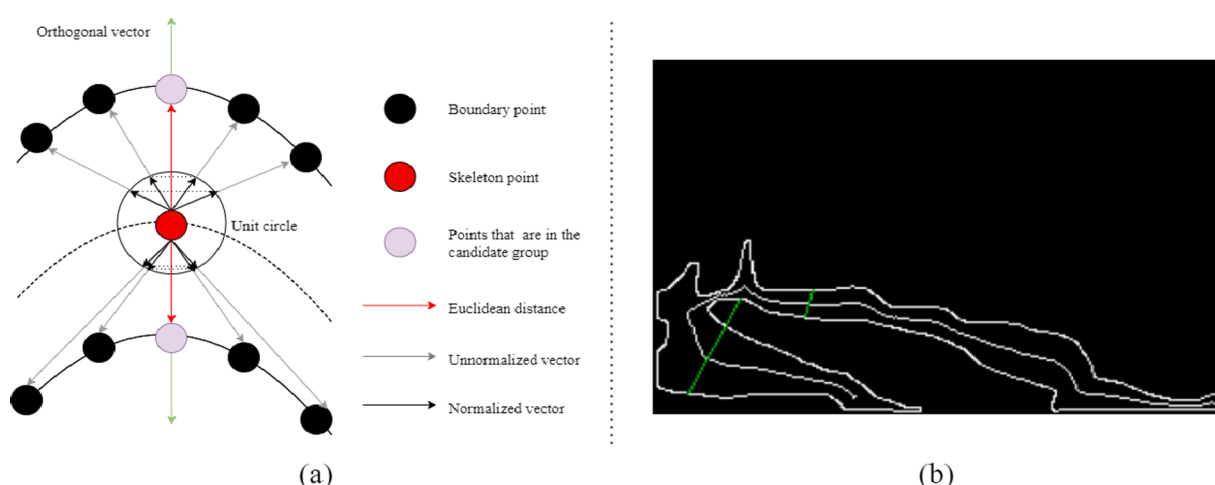


Fig. 2. (a) Illustration of crack width obtained using the orthogonal method. (b) Disadvantages of using orthogonal projection method.

where the index i and j denote the j^{th} pixel of the i^{th} branch. If the weight is below a threshold, α , the branch is deemed unimportant and is pruned from the skeleton. The α value used throughout our experiments is 75. α is determined empirically by testing on public crack datasets. This pruning process is iterated until all the end branches are visited. A comparison between the unpruned skeleton produced by MAT and the pruned skeleton produced by DSE is shown in Fig. 3.

3.2. Intersection removal

After the extraction and pruning of the crack skeleton, the binary image is further processed by removing the intersections and breaking them down into simple linear segments. This preprocessing step is essential as the crack width at the intersection is undefined.

To achieve this, a skeleton is viewed as a graph defined by its nodes and edges. Therefore, an intersection point can be easily found when the degree of a node is greater than two. However, due to the crack's complexity, multiple intersection points are often detected that represent the same intersection in the original binary image. Hence, these intersection points are averaged and floored to obtain a point that represents these multiple intersection points. Then, a circle is fitted at the new intersection point using the midpoint circle algorithm. The radius is initialized at zero and incremented by one until the number of intersections between the perimeter of the circle and the crack boundary exceeds twice the degree of the intersection point. The overall process is shown in Fig. 4.

3.3. Crack orientation

The formation of a crack is due to a local material failure that forms an opening on the pavement surface. Based on the literature review in Section 1, there is no rigorous definition to measure the width of a crack. Therefore, in this paper, the proposed hybrid method finds a pair of points that obtains the shortest distance while being near a skeleton point's orthogonal direction.

To obtain the crack width using the hybrid method, the first step is to obtain the crack propagation direction within a small region. An adaptive kernel size, starting with a size of 5 by 5, is used to obtain pixels at a local region. The kernel size starts with size five, as suggested by the authors of the orthogonal projection method [24]. The local pixels are represented by their local (x, y) coordinates. Due to the nature of cracks, instead of expressing the crack pixels in their original two-dimension coordinate system, the pixels can be expressed with just a one-dimension coordinate system. Hence, Principal Component Analysis (PCA) is used to find the propagation basis vector, $z \in \mathbb{R}^{1 \times 2}$, that projects the 2-dimension coordinate system to a 1-dimension coordinate system. The orthogonal basis vector, $y \in \mathbb{R}^{1 \times 2}$ can be found by solving the null space of the propagation basis vector. The overall process is summarized in Fig. 5. The kernel size is increased by two until the relative difference of the propagation angle between the latter and the prior is less than

0.01. The relative difference threshold is determined empirically based on public crack datasets.

3.4. Crack width

Once the orthogonal basis vector, y is found, the boundary points within a maximal disk, $B \in \mathbb{R}^{N \times 2}$, obtained via the Canny edge detector and the skeleton point, $s \in \mathbb{R}^{1 \times 2}$ are subtracted via Python broadcasting and normalized to obtain vectors of local boundary points with respect to the skeleton point, $B' \in \mathbb{R}^{N \times 2}$, as shown in Equation (3).

$$B' = \frac{B - s}{|B - s|} \quad (3)$$

Then the matrix B' is multiplied with the transpose of the orthogonal basis vector, y , as shown in Equation (4), to obtain a projection coefficient vector, $P \in \mathbb{R}^N$. Each element in P is the projection coefficient of each local boundary point onto the orthogonal vector.

$$P = B' y^T \quad (4)$$

The maximum and minimum of the projection coefficient vector indicate the local boundary points that lie closest to the orthogonal basis vector and opposite of each other. Then, a balancing coefficient β ranging from zero to one is introduced to balance the shortest distance method and orthogonal projection method. A high β value emphasizes the orthogonal projection method and vice versa. Based on the value of β , two groups of candidate points, C_1 and C_2 , are introduced where each group corresponds to each boundary. If the ratio of the local boundary points' projection coefficient to the maximum projection coefficient exceeds the balancing coefficient, then that boundary point is considered a candidate point and is included in C_1 . This process is repeated for C_2 but uses the minimum projection coefficient instead. The process is summarized in Equation (5) and Equation (6). The β value used throughout our experiment is 0.999. It is determined empirically but needs to be a high value, as a low value will ignore the propagation direction of the crack and thus resulting in repeated or skewed measurements.

$$C_1 = B \left[\frac{P}{\max(P)} > \beta \right] \quad (5)$$

$$C_2 = B \left[\frac{P}{\min(P)} > \beta \right] \quad (6)$$

Finally, the crack width is determined based on the shortest Euclidean distance among the candidate points in C_1 and C_2 , as shown in Equation (7). This process is illustrated in Fig. 6, and the flowchart can be seen in Fig. 7. In addition, the pseudocode of the hybrid method is also shown below.

$$\text{Distance} = \sqrt{(x_2 - x_1)^2 + (y_2 - y_1)^2} \quad (7)$$

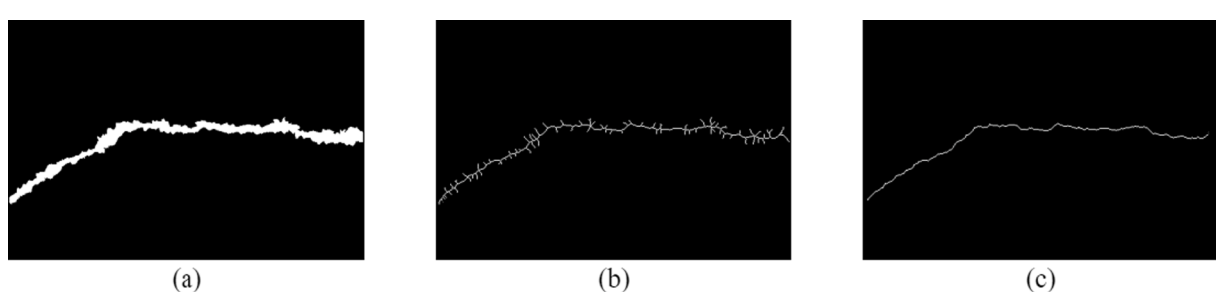


Fig. 3. Comparison of the pruned and unpruned skeleton. (a) Segmented image. (b) Unpruned skeleton obtained via Medial Axis Transform. (c) Pruned skeleton obtained via Discrete Skeleton Evolution.

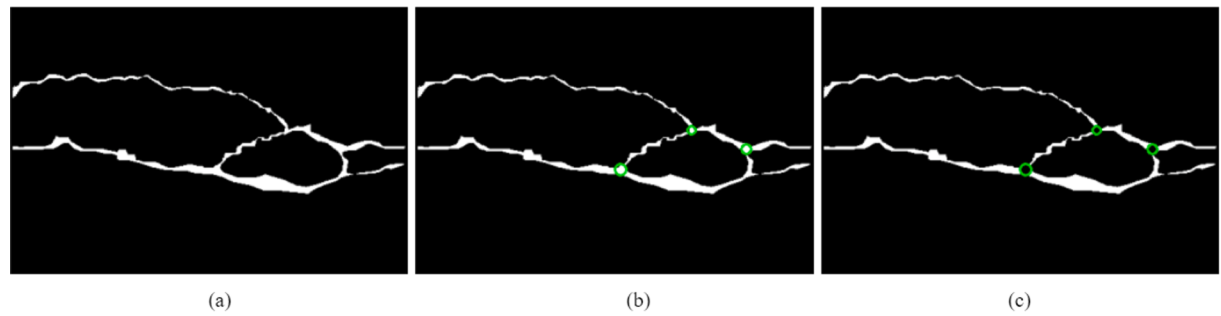


Fig. 4. (a) Original binary image. (b) Intersection points are located by fitting a circle at the intersection point. (c) The pixels in the circle are removed.

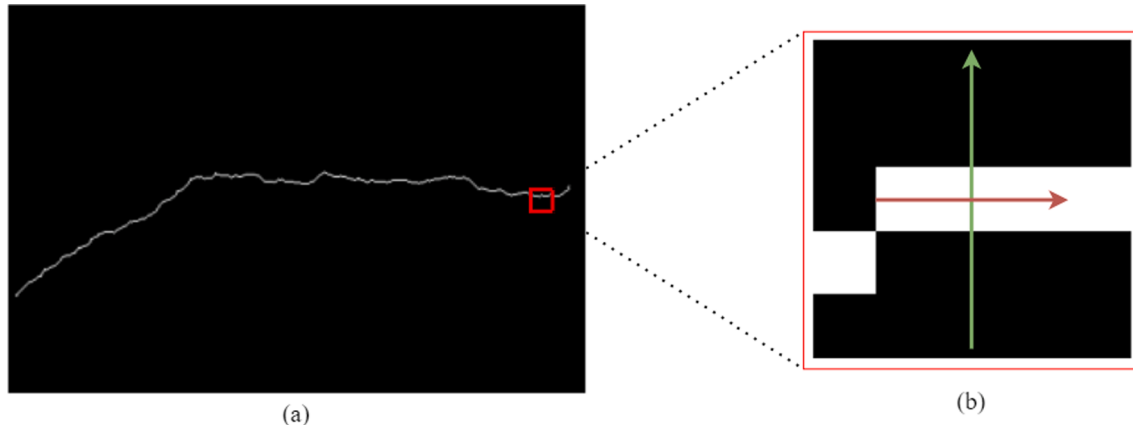


Fig. 5. (a) Crack skeleton after pruning. (b) Local pixels are obtained by a 5 by 5 kernel, where the red and green arrow represents the propagation basis vector and orthogonal basis vector, respectively.

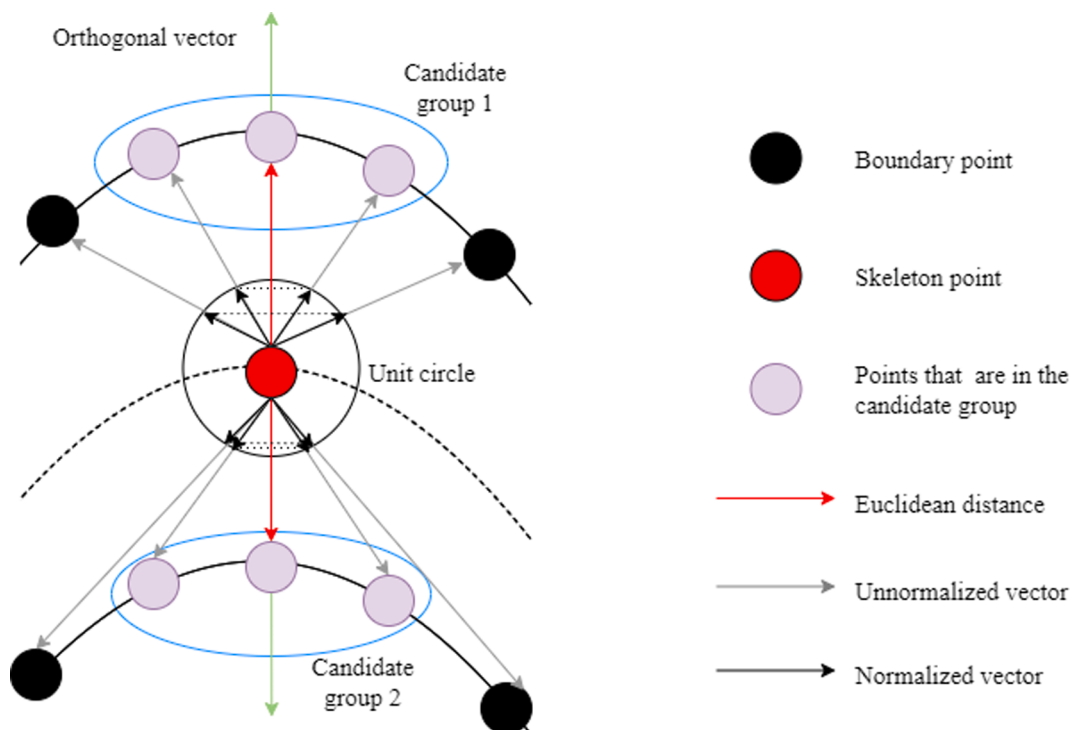


Fig. 6. Illustration of crack width obtained using the hybrid method.

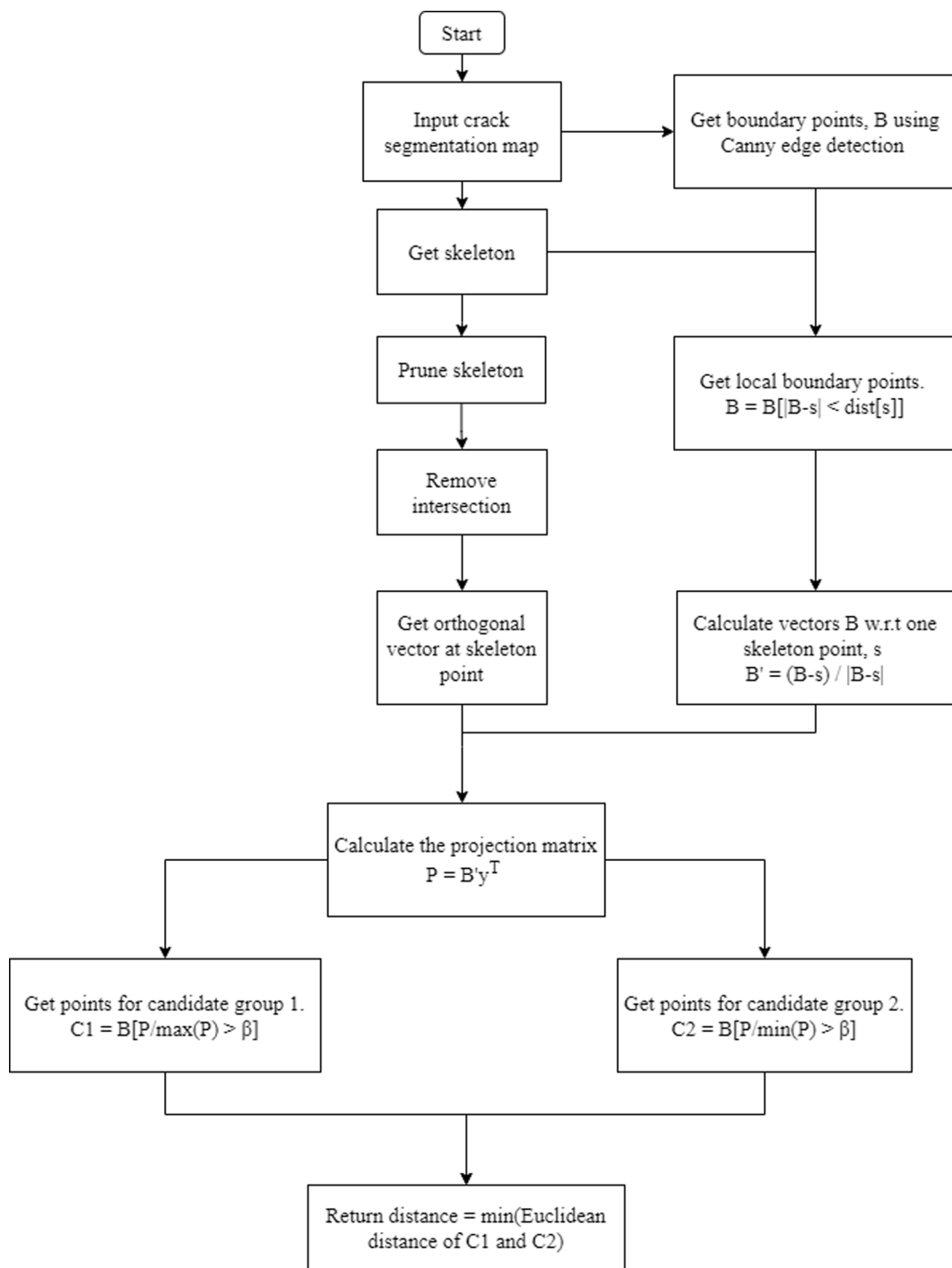


Fig. 7. Hybrid algorithm flow chart.



Fig. 8. Crack segmentation map used for qualitative comparisons.

 Hybrid method(image, s, α , β)

```

1. S, dist = Medial Axis Transform(image)
2. S = DSE(S,dist, $\alpha$ ) # Pruning of unwanted branches
3. S = intersection_removal(S) # Remove bifurcation points
4. B = Canny(image)
5. B = B[|B-s| < dist[s]] # Get local boundary points
6. y = get_orientation(S,s) # Get orthogonal basis vector using PCA
7. B' = (B-s) / |(B-s)| # Normalize the vector B w.r.t s
8. P = B'yT # Obtain the projection coefficients
9. C1 = B[P/max(P) >  $\beta$ ]
10. C2 = B[P/min(P) >  $\beta$ ]
11. distance = min(euclidean_distance(C1,C2))
12. return distance
  
```

The implementation above provides a framework that utilizes vectorization and does not require the crack boundary to be simplified before the crack width is calculated, like the orthogonal projection method [24]. Hence, our proposed framework provides an increase in speed while still obtaining high accuracy, as seen in Section 4.0.

3.5. Image acquisition and database

The data used for quantitative and qualitative comparison of the shortest, orthogonal projection, and hybrid methods are described in this section. We tested these methods quantitatively and qualitatively on real cracks and synthetic cracks.

For the quantitative and qualitative comparisons of real cracks, we tested the methods based on 45 images taken randomly from three databases: our CrackSkel700 and two open datasets, CrackForest [40] and Crack500 [41]. We built the CrackSkel700 dataset, which contains 729 images of resolution 480×320 taken with a smartphone. The images depict the road conditions in Malaysia and are taken perpendicularly to the pavement surface at approximately 1 m above the surface while being stationary. The images are captured using auto mode and the segmented photos are prepared using the LabelMe software [42]. The CrackForest dataset contains 118 crack images of resolution 480×320 captured with a smartphone on the highways of Beijing [40]. The Crack500 dataset contains 500 crack images with a resolution of 2560×1440 and captured on the main campus of Temple University using a smartphone. The authors of Crack500 cropped the images to a size of 640×320 , resulting in 1864 images [41]. Examples of the segmentation images used to test the shortest, orthogonal projection, and hybrid methods are shown in Fig. 8.

For the quantitative and qualitative comparison of synthetic cracks, we generated 30 synthetic cracks based on real crack skeletons that are not included in the 45 images used in our previous test. Then a circle with a known radius is fitted over each skeleton pixel where the center of the circle is the corresponding skeleton pixel. The generated synthetic cracks are used to remove any ambiguities due to subjectivity in measuring the ground truth crack widths. Cracks with varying widths indicate different levels of severity [30–34]. Hence, 30 synthetic cracks are generated, consisting of 18,404 crack width measurements varying from 3 pixels to 61 pixels to simulate cracks with varying widths and crack images taken at different heights. Examples of synthetic cracks used in this experiment are shown in Fig. 9.

4. Results and discussions

We tested the shortest, orthogonal projection and our hybrid method quantitatively and qualitatively based on the data stated in Section 3.5. First, we tested the shortest, orthogonal projection and the hybrid methods quantitatively on real cracks. We selected five images from the databases, randomly chose twenty points from each crack, and measured manually to obtain pixel distances as depicted by the red lines shown in Figs. 10–14. Each point is measured three times, and the

average distance is used as the ground truth. The crack width root mean squared (RMS) error and the absolute pixel deviation are summarized in Table 1 for the shortest, orthogonal projection, and hybrid methods. Cracks 1–5 in Table 1 correspond to Figs. 10–14. The detailed measurements for the cracks shown in Figs. 10–14 using the shortest, orthogonal projection, and hybrid methods are shown in the Appendix. Next, we tested the shortest, orthogonal projection and the hybrid methods qualitatively on public datasets stated in Section 3.5 to understand the differences between these methods. The visual comparison between each method can be seen in Figs. 15 and 16.

In addition, we performed quantitative and qualitative tests on synthetic cracks. The preparation of synthetic cracks is outlined in Section 3.5. The gradient, correlation coefficient, and average absolute deviation of the shortest, orthogonal projection, and hybrid methods are summarized in Table 2. The visual comparison of each method can be seen in Fig. 18.

4.1. Quantitative and qualitative comparisons of real cracks

The crack width root mean square (RMS) error and the absolute pixel deviation for the shortest, orthogonal projection and the hybrid methods are summarized in Table 1. Based on the 100 random measurements shown in Figs. 10–14, the hybrid method obtains the lowest RMS error and the lowest absolute pixel deviation.

To properly understand the severity of the crack, the crack width needs to be measured at every skeleton point to identify possible areas of crack that allow the entry of water and de-icing salt. The entire crack width estimation for the orthogonal projection, shortest and hybrid methods on a real crack is shown in Fig. 15. The maximum crack width for the manual, orthogonal projection, shortest and hybrid methods are 16.72 mm, 33.64 mm, 13.87 mm, and 16.88 mm, respectively, as indicated by the red line in Fig. 15. The hybrid method obtains the maximum crack width estimation closest to the manual measurement. Based on the pavement maintenance guidelines established by the transportation agency in Ireland, the manual, hybrid, and shortest methods recommend that the crack should be repaired using a crack filling strategy with a reservoir, but the orthogonal projection method recommends that the crack should be repaired using a crack filling strategy without a reservoir [33,34]. The orthogonal projection method recommends a different strategy because of the overestimated crack width seen in Fig. 15. Even though the hybrid method and the shortest method proposed a similar crack repair strategy compared to the crack repair strategy suggested by the manual method, the hybrid method outperforms the shortest method as it can measure more distinct crack width measurements, as seen in Fig. 15.

Next, we qualitatively tested the shortest, orthogonal projection and hybrid methods on 45 real crack images stated in Section 3.5 to understand the differences between each method. The qualitative results of each method can be seen in Fig. 16, where the green lines in the figures depict general crack width measurements. The rectangle in blue shown in Fig. 16 marks the location of our analysis globally.

Based on Fig. 16, the shortest method sometimes produces acceptable results but occasionally contains some missing measurements compared to the orthogonal projection and the hybrid methods. This is because the shortest method searches only the boundary pixel nearest to the skeleton point. Therefore, jagged boundaries can easily skew the shortest method, causing repeated measurements at different skeleton points. However, the shortest method produces better results than the orthogonal projection method for cracks that are thin and contain no curved segments, as seen in Fig. 16(b).

The orthogonal projection method produces a distinct crack width measurement at every skeleton point compared to the shortest method. However, this method overestimates the crack width at non-parallel crack boundaries or curved segments of the crack, as seen in Fig. 16. Cracks with unparallel boundaries cause a slight pixel shift in the skeleton and cause the orthogonal vector to skew and select boundary points

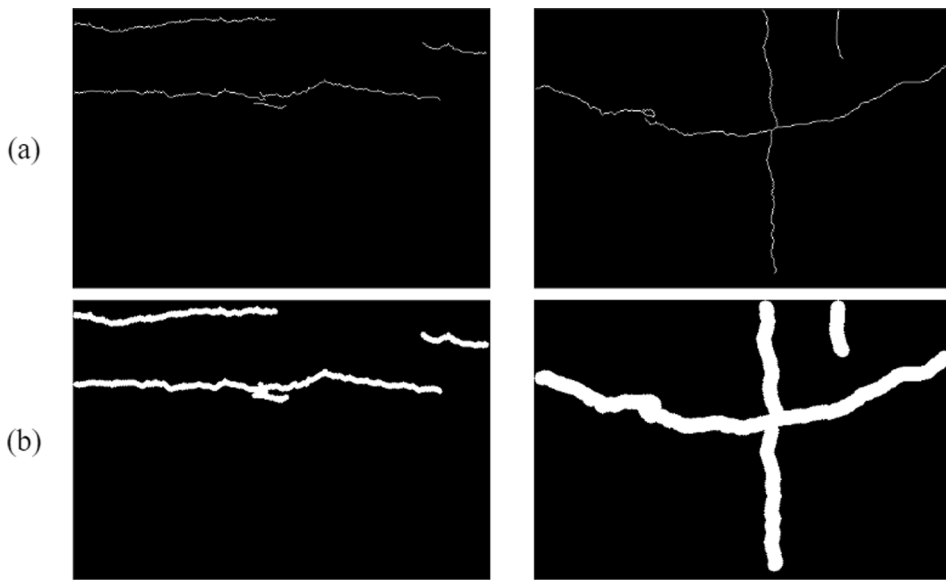


Fig. 9. Simulated cracks with varying widths. (a) Real crack skeletons. (b) Synthetic cracks were generated using a circle with a known radius.

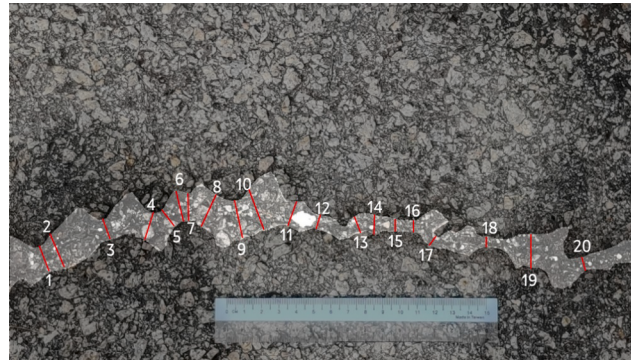


Fig. 10. Linear crack with overlaying measurements.

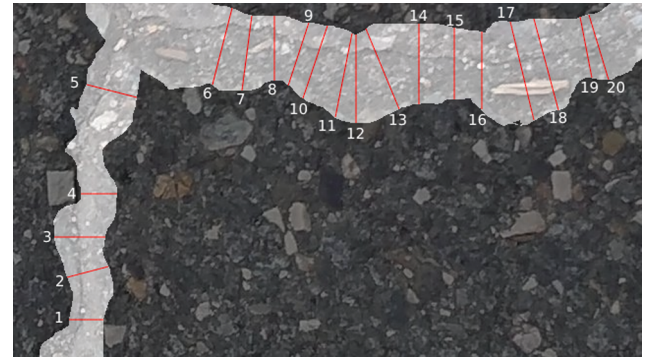


Fig. 12. Block crack with overlaying measurements.

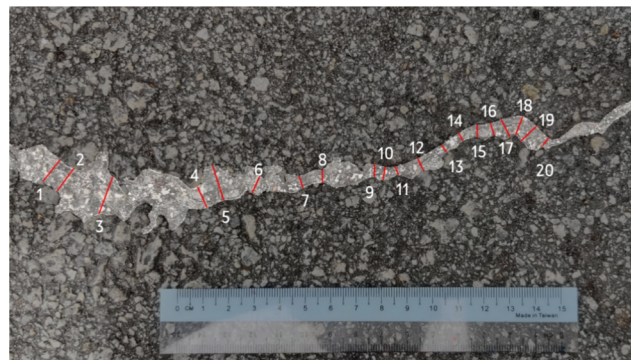


Fig. 11. Linear crack with overlaying measurements.

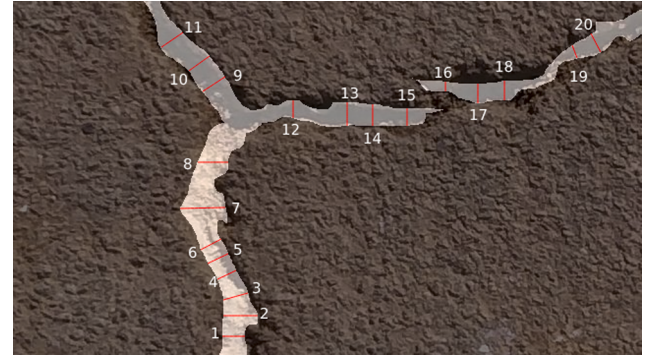


Fig. 13. Block crack with overlaying measurements.

that overestimate the crack width as seen in Fig. 16(a) and 16(b). Furthermore, due to the orthogonal projection's heavy reliance on the orthogonal vector, the orthogonal projection method selects boundary points that lie closest to the orthogonal vector. This causes the method to select points that are not directly in front or behind the skeleton point, as seen in Fig. 16(c).

The hybrid method selects a pair of points that give the shortest distance while being near to the orthogonal vector. By incorporating the propagation direction of the crack, the shortest distance is improved

significantly. The improvement can be seen in Fig. 16(a) and 16(b), where the hybrid method reduces the number of repeated measurements obtained by the shortest method due to jagged boundaries. By incorporating the propagation direction of a crack, the shortest method is more robust to the jagged boundaries of a crack. On the other hand, the hybrid method is more robust to the pixel shift in the skeleton when the crack boundaries are unparallel. Based on Fig. 16(a) and 16(b), the hybrid method produces less skewed measurements when compared to the orthogonal projection method. Furthermore, due to the

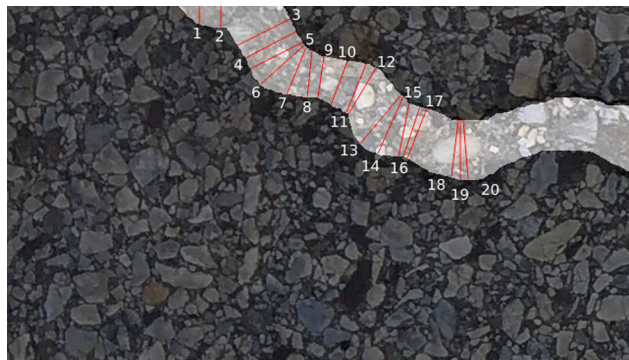


Fig. 14. Linear crack with overlaying measurements.

incorporation of the shortest method, the hybrid method selects points that are directly in front and behind the skeleton point, which fixes the overestimation of the orthogonal projection method seen in Fig. 16(c).

When the crack is linear and slightly curved, the orthogonal projection outperforms the shortest method, as seen in Fig. 16(a). However, when the crack contains fewer jagged edges and unparallel boundaries, the shortest method performs better than the orthogonal projection in Fig. 16(b). When the cracks contain high curvature segments, as seen in Fig. 16(c), the hybrid method outperforms the other methods. Hence, by combining the two methods to produce the hybrid method, we obtain a method that generalizes better to most crack patterns and thus enables the hybrid method to propose more suitable crack repair strategies compared to the orthogonal projection and shortest methods.

4.2. Quantitative and qualitative comparison of simulated cracks

Establishing the ground truth of crack width by manually measuring the cracks may result in some ambiguity as the crack width is often subjective. Therefore, synthetic cracks are generated to evaluate the accuracy and robustness of the three methods rigorously.

The metrics used to measure the performance of each algorithm are the gradient, correlation coefficient between the predicted width and the ground truth, and the average absolute deviation. The gradient of the line measures the overestimation or underestimation of the crack width, where a gradient value higher than 1 indicates overestimation and vice versa. The correlation coefficient measures the accuracy of the measurement where a value of 1 indicates that the predicted width correlates perfectly with the ground truth. The average absolute deviation measures the average difference between the predicted crack width and the ground truth. The metrics for each method are summarized in Table 2.

The predicted width against ground truth graph for the shortest, orthogonal projection, and hybrid methods are shown in Fig. 17. The results in Fig. 17 show that all the methods underestimate several points. This is because the skeleton lies very near to the end points of a crack, as shown in Fig. 19. Therefore, the predicted widths will be lower than the ground truth.

Based on the results in Table 2, the shortest method obtains the highest average absolute deviation and the lowest correlation coefficient compared to the orthogonal projection and hybrid method. The reason for the poor performance is due to the underestimation of crack width, as indicated by the gradient value. Based on Fig. 18, the shortest method obtains repeated measurements at different skeleton points, leading to the underestimation of crack width. The jagged boundaries cause the

Table 1
Statistics of the shortest, orthogonal projection and hybrid method on real cracks.

Crack	Shortest RMS (px)	OP RMS (px)	Hybrid RMS (px)	Shortest absolute deviation (px)	OP absolute deviation (px)	Hybrid absolute deviation (px)
1	3.324	1.986	0.939	2.093	1.579	0.728
2	5.172	1.951	1.013	2.245	1.099	0.812
3	6.066	4.476	1.585	4.022	3.312	1.145
4	4.116	1.412	0.671	1.958	1.059	0.453
5	3.496	1.988	0.794	2.282	1.794	0.522
Average	4.434	2.363	1.000	2.520	1.768	0.732

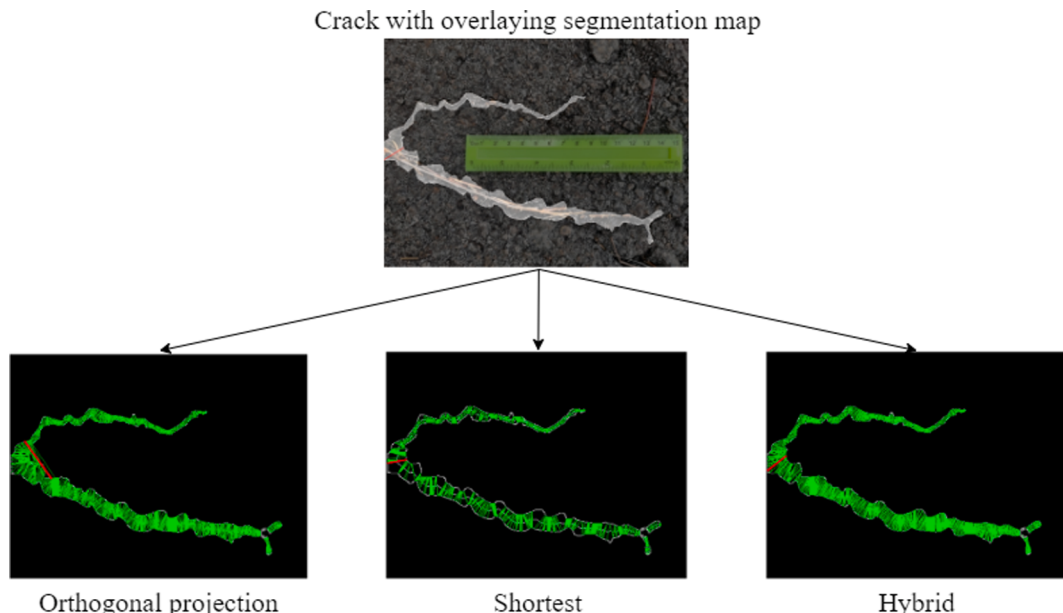


Fig. 15. Entire crack width estimation using orthogonal projection, shortest and hybrid methods.

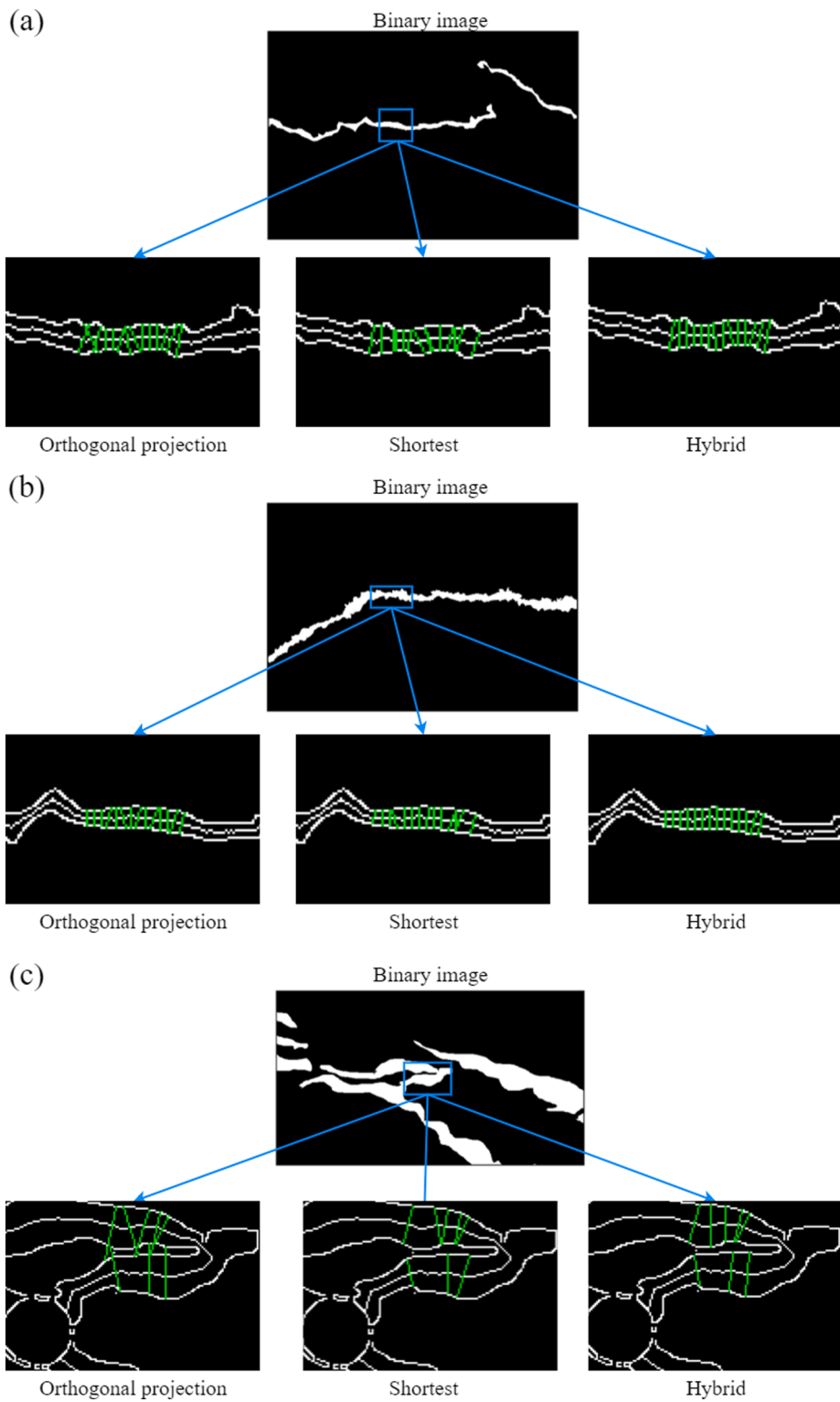


Fig. 16. Visual comparison of real cracks using orthogonal projection, shortest and hybrid methods.

shortest method to ignore other boundary points and thus causing repeated measurements, as seen in Fig. 18. The repeated measurement then leads to the underestimation of crack width.

The orthogonal projection method improves the crack width estimation compared to the shortest method as it obtains a higher correlation coefficient and lower absolute deviation. Based on Table 2, the orthogonal projection method overestimates the crack width. The orthogonal projection method obtains skewed measurements when

there is a pixel shift in the skeleton due to unparallel crack boundaries, as seen in Fig. 18(a) and 18(b). The presence of pixel shift skews the orthogonal vector and produces skewed measurements when using the orthogonal projection. In addition, the orthogonal projection method severely overestimates the crack width when the crack contains high curvature, as seen in Fig. 18(c). When the crack has high curvature, the orthogonal projection method selects points that are not directly in front or behind the skeleton point and causes an overestimation of crack

Table 2

Summarized results of the shortest method, orthogonal projection method, and hybrid method on simulated cracks.

Method	Gradient	Correlation coefficient, R	Average absolute deviation (px)
Shortest	0.923	0.882	2.753
Orthogonal Projection	1.048	0.947	2.261
Hybrid method	1.011	0.955	1.769

width. This overestimation is due to the strict selection of boundary points that lie closest to the orthogonal vector.

Based on Table 2, the hybrid method obtains the least average absolute deviation and highest correlation coefficient. The improvement is indicated by reducing overestimation and underestimation of crack width when compared to the orthogonal projection method and the shortest method, respectively. Based on Fig. 18, the hybrid method contains more distinct measurements at different skeleton points of the crack as compared to the shortest method. Incorporating the crack propagation direction into the shortest method, the shortest method is improved significantly by reducing the number of repeated measurements. On the other hand, the hybrid method is more robust to pixel shift in the skeleton as the hybrid method produces less skewed measurements when compared to the orthogonal projection method, as seen in Fig. 18(a) and 18(b). Furthermore, as the hybrid method selects a pair of points that provide the shortest distance, therefore the hybrid method chooses points that are directly in front and behind the skeleton point, as seen in Fig. 18(c). Hence, we show that the hybrid method fixes the overestimation and underestimation of the orthogonal projection method and the shortest method.

Based on the qualitative comparison shown in Fig. 18, the shortest method performs better than the orthogonal projection method when the crack contains fewer jagged edges, as seen in Fig. 18(a). On the other

hand, the orthogonal projection method performs much better than the shortest method when the crack contains slightly curved sections, as seen in Fig. 18(b). However, when the cracks contain high curvature, the hybrid method outperforms both the orthogonal projection and the shortest method, as seen in Fig. 18(c).

5. Conclusion

In conclusion, we developed a new hybrid method for measuring crack widths by combining the shortest and orthogonal projection methods. The hybrid method identifies a pair of points closest to the skeleton point while being close to the orthogonal vector. We tested our hybrid method against the shortest method and the orthogonal projection method quantitatively and qualitatively on real and synthetic cracks taken from our CrackSkel700 dataset and two open datasets, CrackForest and Crack500. One hundred manual measurements are taken from five images chosen randomly in the datasets to perform quantitative test on the shortest, orthogonal projection, and hybrid methods. The average RMS error for the shortest, orthogonal projection and hybrid method is 4.434, 2.363, and 1.000 pixels, respectively. Meanwhile, the average absolute deviation for the shortest, orthogonal projection and hybrid method is 2.520, 1.768, and 0.732 pixels, respectively.

To eliminate any ambiguity due to subjective crack width measurements, we generated 30 synthetic cracks with varying crack widths of 3 pixels to 61 pixels to simulate cracks with varying crack width and crack images taken at different heights. Each method's performance is measured using the gradient, correlation coefficient, and average absolute deviation. Based on the performance of each method on the synthetic data, the hybrid method obtains the least average absolute deviation of 1.769 and the highest correlation coefficient of 0.956 when compared to the shortest method and the orthogonal projection method.

To understand the differences between each method, we compared

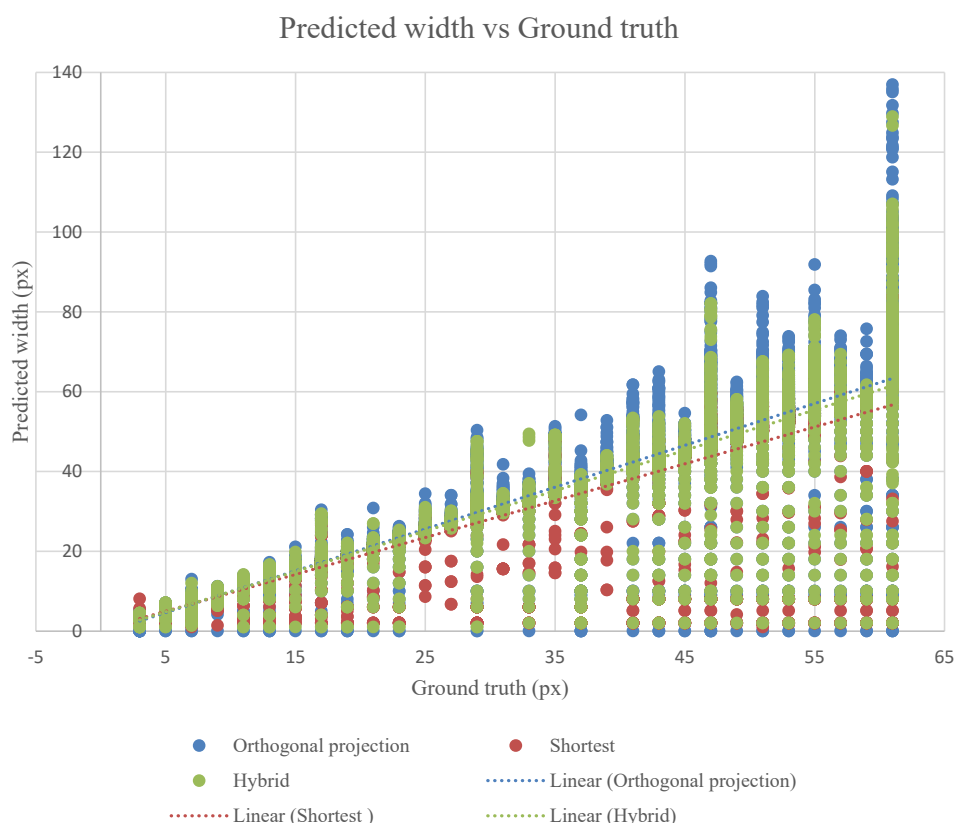


Fig. 17. Predicted width vs ground truth measurements on synthetic cracks for the orthogonal projection, shortest and hybrid methods.

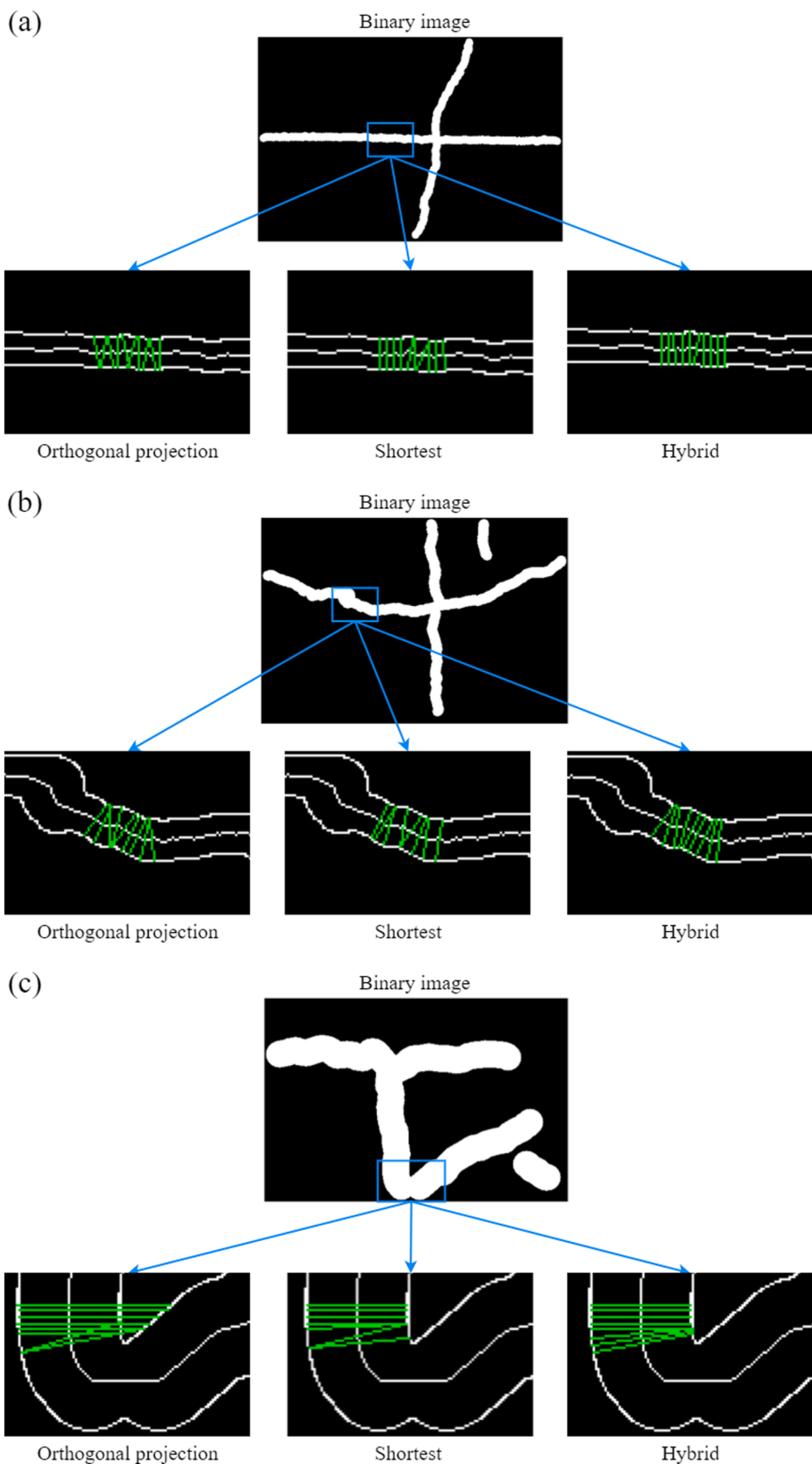


Fig. 18. Visual comparison on synthetic cracks using orthogonal projection, shortest and hybrid methods.

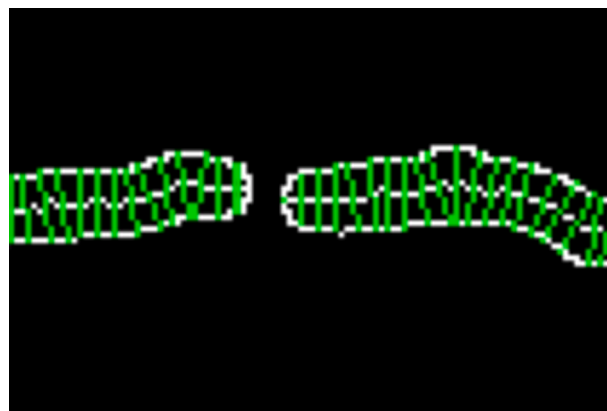


Fig. 19. Outlier crack width estimation.

the shortest, orthogonal projection, and hybrid methods qualitatively on real and synthetic cracks. The incorporation of propagation direction with the shortest method improves the shortest method significantly by reducing the number of repeated measurements. On the other hand, the hybrid method reduces the overestimation of crack width obtained by the orthogonal projection method at non-parallel crack boundaries and cracks with high curvature. Hence, we show that the hybrid method generalizes better than the shortest and orthogonal projection methods. Based on the quantitative and qualitative tests shown, the hybrid method can be used to rank the severity of cracks so that the transport agencies can address and repair pavements that are severely damaged first.

Appendix. Detailed measurements of real cracks

Table A: Comparison of orthogonal projection, shortest and hybrid measurement methods for crack shown in Fig. 10.

Point	Average distance (px)	OP measurement (px)	Shortest measurement (px)	Hybrid measurement (px)
1	43.763	44.721	43.081	43.829
2	58.343	58.821	48.877	58.830
3	34.513	34.482	33.956	34.482
4	46.613	46.615	44.272	46.818
5	33.090	33.951	32.650	33.242
6	50.023	51.244	47.170	50.596
7	44.333	46.097	45.000	45.177
8	55.550	58.523	54.037	55.973
9	61.977	56.851	59.908	60.415
10	69.897	72.007	60.374	71.196
11	42.453	43.681	41.000	43.931
12	22.513	24.000	22.361	22.361
13	27.870	26.832	25.962	26.833
14	30.917	29.614	28.178	30.414
15	20.057	22.000	21.023	22.000
16	18.777	17.204	19.026	20.000
17	17.923	21.840	16.643	17.888
18	16.333	18.000	17.464	18.000
19	53.333	54.000	52.611	53.758
20	22.023	23.259	20.881	22.472

Table B: Comparison of orthogonal projection, shortest and hybrid measurement methods for crack shown in Fig. 11.

Point	Average distance (px)	OP measurement (px)	Shortest measurement (px)	Hybrid measurement (px)
1	42.923	43.841	42.521	43.139
2	44.050	45.222	43.829	44.102
3	62.830	70.662	49.739	64.070
4	36.780	37.643	36.401	37.336
5	58.433	58.000	39.812	58.694
6	28.590	28.653	27.459	28.178

(continued on next page)

(continued)

Point	Average distance (px)	OP measurement (px)	Shortest measurement (px)	Hybrid measurement (px)
7	20.203	19.925	19.313	19.924
8	20.220	22.000	22.000	22.000
9	20.110	21.000	21.000	21.000
10	20.650	22.000	20.025	22.000
11	14.157	14.560	14.140	15.133
12	21.620	21.843	21.541	22.472
13	14.300	14.422	13.601	14.422
14	14.047	14.422	13.892	14.422
15	20.083	21.000	20.025	21.000
16	20.937	21.377	21.095	21.378
17	31.450	32.985	29.154	33.541
18	32.140	33.000	31.385	32.558
19	34.950	34.409	33.422	33.971
20	15.987	16.971	14.866	18.028

Table C: Comparison of orthogonal projection, shortest and hybrid measurement methods for crack shown in Fig. 12.

Point	Average distance (px)	OP measurement (px)	Shortest measurement (px)	Hybrid measurement (px)
1	35.007	36.000	34.058	36.000
2	44.017	42.942	42.485	42.485
3	52.067	52.000	50.488	51.000
4	37.033	36.000	36.000	36.000
5	52.447	52.953	52.469	52.953
6	80.737	81.608	80.062	80.231
7	76.500	86.977	70.406	79.000
8	65.580	74.330	67.000	67.000
9	66.497	66.098	62.642	65.145
10	78.470	80.212	70.214	78.230
11	87.257	92.130	80.777	88.102
12	89.777	98.061	83.815	94.726
13	88.390	95.000	86.874	86.815
14	79.667	82.000	82.000	82.000
15	71.667	76.538	71.000	72.339
16	79.167	83.744	69.231	79.429
17	102.460	105.574	97.744	102.961
18	94.483	96.603	74.686	94.366
19	62.660	64.846	61.660	62.801
20	68.643	70.000	66.030	69.000

Table D: Comparison of orthogonal projection, shortest and hybrid measurement methods for crack shown in Fig. 13.

Point	Average distance (px)	OP measurement (px)	Shortest measurement (px)	Hybrid measurement (px)
1	23.000	23.000	22.022	23.000
2	35.000	31.305	26.926	35.000
3	26.567	26.683	26.000	26.305
4	21.547	21.840	20.881	21.471
5	23.180	23.086	22.361	23.259
6	23.260	23.021	22.022	23.259
7	46.000	48.765	30.000	46.043
8	31.000	29.411	28.406	29.547
9	26.997	28.178	26.627	27.202
10	26.003	27.018	25.000	25.495
11	27.553	26.926	26.420	27.459
12	17.417	17.000	17.000	17.000
13	22.887	24.000	24.000	24.000
14	21.333	23.537	22.203	23.000
15	17.000	18.440	18.000	18.110
16	9.780	11.180	10.049	10.049
17	19.220	20.396	20.000	20.000
18	19.443	20.000	19.698	20.000
19	14.503	15.524	14.142	14.765
20	21.253	21.024	20.591	21.095

Table E: Comparison of orthogonal projection, shortest and hybrid measurement methods for crack shown in Fig. 14.

Point	Average distance (px)	OP measurement (px)	Shortest measurement (px)	Hybrid measurement (px)
1	17.943	19.235	15.811	17.720
2	21.500	22.805	22.000	22.091
3	61.030	64.413	49.193	62.801
4	57.453	58.592	57.697	57.697

(continued on next page)

(continued)

Point	Average distance (px)	OP measurement (px)	Shortest measurement (px)	Hybrid measurement (px)
5	59.433	60.374	57.697	59.540
6	60.800	63.253	56.302	60.811
7	51.873	54.231	49.335	52.801
8	47.883	44.922	44.272	45.891
9	42.650	45.000	42.426	42.755
10	48.283	49.648	46.487	48.301
11	54.107	55.227	50.990	53.852
12	54.470	57.245	53.852	54.378
13	64.733	66.648	62.650	64.443
14	64.017	65.000	58.181	63.906
15	55.153	56.320	53.759	54.918
16	52.480	53.451	52.886	52.886
17	54.173	55.362	53.141	54.083
18	58.710	60.729	57.706	59.304
19	59.403	62.936	60.299	61.131
20	61.347	62.000	61.204	62.000

References

- [1] M. Elkashef, R.C. Williams, E. Cochran, Investigation of fatigue and thermal cracking behavior of rejuvenated reclaimed asphalt pavement binders and mixtures, *Int. J. Fatigue* 108 (2018) 90–95, <https://doi.org/10.1016/j.ijfatigue.2017.11.013>.
- [2] D. Zhang, Q. Zou, H. Lin, X. Xu, L.i. He, R. Gui, Q. Li, Automatic pavement defect detection using 3D laser profiling technology, *Autom. Constr.* 96 (2018) 350–365, <https://doi.org/10.1016/j.autcon.2018.09.019>.
- [3] K. Zhang, H.D. Cheng, B. Zhang, Unified Approach to Pavement Crack and Sealed Crack Detection Using Preclassification Based on Transfer Learning, *J. Comput. Civil Eng.* 32 (2) (2018) 04018001, [https://doi.org/10.1061/\(ASCE\)CP.1943-5487.0000736](https://doi.org/10.1061/(ASCE)CP.1943-5487.0000736).
- [4] J. Liu, X.u. Yang, S. Lau, X. Wang, S. Luo, V.-S. Lee, L. Ding, Automated pavement crack detection and segmentation based on two-step convolutional neural network, *Comput.-Aided Civ. Infrastruct. Eng.* 35 (11) (2020) 1291–1305.
- [5] J. Lee, B. Nam, M. Abdel-Aty, Effects of Pavement Surface Conditions on Traffic Crash Severity, *J. Transp. Eng.* 141 (10) (2015) 04015020, [https://doi.org/10.1061/\(ASCE\)TE.1943-5436.0000785](https://doi.org/10.1061/(ASCE)TE.1943-5436.0000785).
- [6] C.V. Dung, L.D. Anh, Autonomous concrete crack detection using deep fully convolutional neural network, *Autom. Constr.* 99 (2019) 52–58, <https://doi.org/10.1016/j.autcon.2018.11.028>.
- [7] S. Zhou, W. Song, Concrete roadway crack segmentation using encoder-decoder networks with range images, *Autom. Constr.* 120 (2020) 103403, <https://doi.org/10.1016/j.autcon.2020.103403>.
- [8] A. Zhang, K.C.P. Wang, B. Li, E. Yang, X. Dai, Y.i. Peng, Y. Fei, Y. Liu, J.Q. Li, C. Chen, Automated Pixel-Level Pavement Crack Detection on 3D Asphalt Surfaces Using a Deep-Learning Network, *Comput.-Aided Civ. Infrastruct. Eng.* 32 (10) (2017) 805–819.
- [9] Y. Liu, J. Yao, X. Lu, R. Xie, L. Li, DeepCrack: A deep hierarchical feature learning architecture for crack segmentation, *Neurocomputing* 338 (2019) 139–153, <https://doi.org/10.1016/j.neucom.2019.01.036>.
- [10] H. Li, D. Song, Y.u. Liu, B. Li, Automatic Pavement Crack Detection by Multi-Scale Image Fusion, *IEEE Trans. Intell. Transp. Syst.* 20 (6) (2019) 2025–2036, <https://doi.org/10.1109/TITS.2018.2856928>.
- [11] S.L.H. Lau, E.K.P. Chong, X. Yang, X. Wang, Automated Pavement Crack Segmentation Using U-Net-based Convolutional Neural Network, p. arXiv: 2001.01912. [Online]. Available: <https://ui.adsabs.harvard.edu/abs/2020arXiv200101912>.
- [12] M.R. Jahanshahi, S.F. Masri, A new methodology for non-contact accurate crack width measurement through photogrammetry for automated structural safety evaluation, *Smart Mater. Struct.* 22 (3) (2013) 035019, <https://doi.org/10.1088/0964-1726/22/3/035019>.
- [13] X. Weng, Y. Huang, W. Wang, Segment-based pavement crack quantification, *Autom. Constr.* 105 (2019) 102819, <https://doi.org/10.1016/j.autcon.2019.04.014>.
- [14] W. Wang, M. Wang, H. Li, H. Zhao, K. Wang, C. He, J. Wang, S. Zheng, J. Chen, Pavement crack image acquisition methods and crack extraction algorithms: A review, *J. Traff. Transport. Eng. (Engl. Ed.)* 6 (6) (2019) 535–556, <https://doi.org/10.1016/j.jtte.2019.10.001>.
- [15] T. Yamaguchi, S. Hashimoto, Practical image measurement of crack width for real concrete structure, *Electron. Commun. Jpn.* 92 (10) (2009) 1–12, <https://doi.org/10.1002/ecj.10151>.
- [16] T. Barkavi, N. Chidambarathanu, Processing Digital Image for Measurement of Crack Dimensions in Concrete, *Civil Eng. Infrastruct. J.* 52 (1) (2019) 11–22, <https://doi.org/10.22059/ceij.2019.246397.1444>.
- [17] X. Yang, H. Li, Y. Yu, X. Luo, T. Huang, X.u. Yang, Automatic Pixel-Level Crack Detection and Measurement Using Fully Convolutional Network, *Comput.-Aided Civ. Infrastruct. Eng.* 33 (12) (2018) 1090–1109.
- [18] H. Oliveira, P.L. Correia, Automatic Road Crack Detection and Characterization, *IEEE Trans. Intell. Transp. Syst.* 14 (1) (2013) 155–168, <https://doi.org/10.1109/TITS.2012.2208630>.
- [19] A. Ji, X. Xue, Y. Wang, X. Luo, W. Xue, An integrated approach to automatic pixel-level crack detection and quantification of asphalt pavement, *Autom. Constr.* 114 (2020) 103176, <https://doi.org/10.1016/j.autcon.2020.103176>.
- [20] C. Liu, C.-S. Tang, B. Shi, W.-B. Suo, Automatic quantification of crack patterns by image processing, *Comput. Geosci.* 57 (2013) 77–80, <https://doi.org/10.1016/j.cageo.2013.04.008>.
- [21] C. Benz, V. Rodehorst, Model-based Crack Width Estimation using Rectangle Transform, in: 2021 17th International Conference on Machine Vision and Applications (MVA), 25–27 July 2021 2021, pp. 1–5. <https://doi.org/10.23919/MVA51890.2021.9511346>.
- [22] T. Nishikawa, J. Yoshida, T. Sugiyama, Y. Fujino, Concrete Crack Detection by Multiple Sequential Image Filtering, *Comput.-Aided Civ. Infrastruct. Eng.* 27 (1) (2012) 29–47, <https://doi.org/10.1111/j.1467-8667.2011.00716.x>.
- [23] L. Duan, H. Geng, J. Zeng, J. Pang, and Q. Huang, Fast and Accurately Measuring Crack Width via Cascade Principal Component Analysis, in: Presented at the Proceedings of the ACM Multimedia Asia, Beijing, China, 2019. [Online]. Available: <https://doi.org/10.1145/3338533.3366578>.
- [24] S. Qiu, W. Wang, S. Wang, K.C.P. Wang, Methodology for accurate AASHTO PP67-10-Based cracking quantification using 1-mm 3D pavement images, *J. Comput. Civil Eng.* 31 (2) (2017) 04016056, [https://doi.org/10.1061/\(ASCE\)CP.1943-5487.0000627](https://doi.org/10.1061/(ASCE)CP.1943-5487.0000627).
- [25] F. Ni, J. Zhang, Z. Chen, Zernike-moment measurement of thin-crack width in images enabled by dual-scale deep learning, *Comput.-Aided Civ. Infrastruct. Eng.* 34 (5) (2019) 367–384.
- [26] B. Kim, S. Cho, Image-based concrete crack assessment using mask and region-based convolutional neural network, *Struct. Control Health Monit.* 26 (8) (2019) e2381, <https://doi.org/10.1002/stc.2381>.
- [27] M. Payab, R. Abbasina, M. Khanzadi, A Brief Review and a New Graph-Based Image Analysis for Concrete Crack Quantification, *Arch. Comput. Methods Eng.* 26 (2) (2019) 347–365, <https://doi.org/10.1007/s11831-018-9263-6>.
- [28] W. Wang, A. Zhang, K.C.P. Wang, A.F. Ibrahim, S. Qiu, Pavement Crack Width Measurement Based on Laplace's Equation for Continuity and Unambiguity, *Comput.-Aided Civ. Infrastruct. Eng.* 33 (2) (2018) 110–123.
- [29] G. Griffiths, N. Thom, *Concrete Pavement Design Guidance Notes*, Taylor & Francis Group, 2019.
- [30] J.E.H. Jeffery, R. Roesler, Alexander S. Brand, S. Tyson (Ed.), *Continuously Reinforced Concrete Pavement Manual*, Federal Highway Administration, United States, 2016.
- [31] J. Poulsom, *Concrete Pavement Maintenance Manual*, Highways England Safety, Engineering and Standards, England, 2021.
- [32] Maintenance Technical Advisory Guide (TAG): Volume I – Flexible Pavement Preservation, Second Edition [CalTrans, 2008], (in English), Tech Report 2008. (Online). Available: <https://rosap.ntl.bts.gov/view/dot/27612>.
- [33] Pavement Assessment, Repair and Renewal Principles, Transport Infrastructure Ireland (TII) Publications, Ireland, 2020, pp. 108.
- [34] Crack Sealing and Joint Repair Systems, Transport Infrastructure Ireland (TII) Publications, Ireland, 2019, pp. 53.
- [35] B. Durix, S. Chambois, K. Leonard, J.-L. Mari, G. Morin, The Propagated Skeleton: A Robust Detail-Preserving Approach, Cham, 2019: Springer International Publishing, in: *Discrete Geometry for Computer Imagery*, pp. 343–354.
- [36] R. Ogniewicz, M. Ilg, Voronoi skeletons: theory and applications, in: *Proceedings 1992 IEEE Computer Society Conference on Computer Vision and Pattern Recognition*, 15–18 June 1992 1992, pp. 63–69. <https://doi.org/10.1109/CVPR.1992.223226>.
- [37] A. Leborgne, J. Mille, L. Tougne, Noise-resistant Digital Euclidean Connected Skeleton for graph-based shape matching, *J. Vis. Commun. Image Represent* 31 (2015) 165–176, <https://doi.org/10.1016/j.jvcir.2015.06.005>.

- [38] H. Blum, Biological shape and visual science (part I), *J. Theor. Biol.* 38 (2) (1973) 205–287, [https://doi.org/10.1016/0022-5193\(73\)90175-6](https://doi.org/10.1016/0022-5193(73)90175-6).
- [39] X. Bai, L.J. Latecki, Discrete Skeleton Evolution, Berlin, Heidelberg, 2007: Springer Berlin Heidelberg, in: *Energy Minimization Methods in Computer Vision and Pattern Recognition*, pp. 362–374.
- [40] Y. Shi, L. Cui, Z. Qi, F. Meng, Z. Chen, Automatic Road Crack Detection Using Random Structured Forests, *IEEE Trans. Intell. Transp. Syst.* 17 (12) (2016) 3434–3445, <https://doi.org/10.1109/TITS.2016.2552248>.
- [41] F. Yang, L. Zhang, S. Yu, D. Prokhorov, X. Mei, H. Ling, Feature Pyramid and Hierarchical Boosting Network for Pavement Crack Detection, pp. arXiv: 1901.06340. [Online]. Available: <https://ui.adsabs.harvard.edu/abs/2019arXiv190106340Y>.
- [42] W. Kentaro, Labelme: Image Polygonal Annotation with Python. <https://doi.org/10.5281/zenodo.5711226>.